DESIGN OPTIMIZATION AND DYNAMIC TESTING OF CFRP FOR HELICOPTER LOADING HANGER (AEROSPACE)

Table of Contents

Abstract

Keywords

1. **Introduction**
2. **Methodology**

2.1. CAD Modeling

2.2. Multiphysics Analysis

2.3. Design Optimization Approach

2.4. CFRP Samples

2.5. Shock Tube Experiment Setup

2.6. Material Test System (MTS)

3. **Results and discussion**

3.1. Design Optimization Results

3.2. Shock Tube Experiment Results

3.3. Material Test System (MTS) Results

3.4. Finite Element Simulations Results

4. **Conclusion**
5. **References**

 DOI: https://doi.org/10.1016/B978-0-12-817899-7.00005-8

DESIGN OPTIMIZATION AND DYNAMIC TESTING OF CFRP FOR HELICOPTER LOADING HANGER (AEROSPACE)

Abstract

This chapter presents the Multiphysics technique applied in the design optimization of a loading hanger for an aerial crane. In this study, design optimization is applied on the geometric modelling of a part being used in an aerial crane operation. A set of dimensional and loading requirements are provided. Various geometric models are built using SolidWorks® Computer Aided Design (CAD) Package. In addition, Finite Element Method (FEM) is applied to study these geometric models using ANSYS® Multiphysics software. Appropriate material is chosen based on the strength to weight ratio. Efforts are made to optimize the geometry to reduce the weight of the part. Further the chosen carbon fiber reinforced polymers (CFRPs) quasi-isotropic shell structures are analyzed under the influence of dynamic loading. The quasi-isotropic CFRPs shell specimens are fabricated using Multipreg E720 laminates. In this study, the dynamic loading is generated using shock waves in a shock tube experimental setup. The strain and pressure data is collected from the experiments. Additional tests are carried out using Material Test System (MTS) for both tensile and flexural response of CFRPs. Results obtained from experiments are compared with numerical simulations. The numerical simulation and experimental results are found to be in good agreement. Based on the achieved results, conclusions are drawn.

Keywords: Design Optimization, Geometric Modeling, Finite Element Method, CFRPs, Dynamic Loading, Shock Waves, MTS

1. INTRODUCTION

Aerial cranes are being used in the wide variety of applications such as in construction, transport, emergency, military etc. [1][2][3]. Fig. 1(a) shows an aerial crane operation. Aerial crane operation involves helicopter, loading hanger and the lifted weight. Loading hanger is comprised of parts, such as loading line, attachment plate, slings, etc. Fig. 1(b) shows a close-up view of the loading hanger [4].

Figure 1 (a) here	Figure 1 (b) here

Figure 1 (a): Aerial crane operation is shown	Figure 1 (b): A zoom in view of loading hanger is shown comprising of three main segments, loading line from the helicopter, the attachment plate and slings to attach the weight [5].

In this work, focus is on the loading hanger. The loading hanger is connected between helicopter and the load. This connection is activated using electromagnetic switch, which can be detached on unloading or emergency in case of unstable helicopter flight. The objective here is to design this part, select appropriate material, use Multiphysics tools for optimization, test material against dynamic loading in shock tube experimental setup and after shock impact analyze chosen material specimens for any changes in tensile and flexural properties in Material Testing System (MTS). This work presents five phases, which includes (1) geometric modeling, (2) material selection and (3) design optimization (4) shock tube experiment (5) MTS.

The geometric modelling phase begins with a sketch of the attachment plate. Fig. 2(a) and 2(b) show the top and side views of the attachment plate based on pre-set design requirements. A set of requirements is provided to enclose a physical problem [6][7]. There are four sling holes surrounded by an attachment area. Each sling hole has a diameter of three centimeters. In addition to that, each hole needs to be thirty centimeters from the center of the attachment plate and equidistant from each other. The center area is for joining the attachment plate with the helicopter. It is also pre-set to 100 cm^2. Only requirement here is that this area should be axisymmetric to the center of the attachment plate. The helicopter maximum loading capacity is up to one metric ton (1000 Kg).

Figure 2 (a) here	Figure 2 (b) here
(a) Top view is shown	(b) side view is shown

Figure 2. The attachment plate with pre-set dimensions' requirements.

Material selection phase is the choosing of an appropriate material for the attachment plate. It is desired that the designed part is efficient and safe. In this case, strength and stiffness are both important. In this work, appropriate material is chosen from a list of available materials. Another important selection criterion is strength to weight ratio. The factor of safety is considered to be three in the selection process [5][8].
The optimization phase includes modifications in the geometry of the attachment plate while fulfilling all of the above given requirements. The focus is on the structural stresses and displacements. The aim is to reduce the weight of the attachment plate.
The composite materials are increasingly used in a number of applications, requiring high strength and light weight properties. With the increase in usage of composites, it is also becoming essential to study them [9]. Researchers have tested various materials subjected to shock wave [10]. Usually, such experiments are carried out using explosives submerged in water [11] [12]. The test specimens are placed at different distances to control the intensity of shock waves [13] [14]. This method is both expensive and potentially dangerous and requires careful planning [11][15]. In addition, complicated calculations and estimations are required to analyze the results. Another method is based on creating shock waves in a shock tube [16]. Such method has considerable advantages in comparison to earlier methods [17][18]. In this method, either a solid projectile or a high pressure fluid is injected into a tube containing liquid instantaneously. This generates a shock wave which propagates along the tube. A test specimen subjected to the shock wave can be placed along the tube. The intensity of shock wave is controlled using velocity of entering projectile or the pressure of fluid. Further control can be added using a T-junction in the tube [17]. Pressure transducers and strain gauges can be placed along the tube for the collection of data. The shock tube experimental setup used in this study is given in Section 2.5.

2. METHODOLOGY

The methodology followed in this study involves development of CAD models using SoildWorks® [19] and Multiphysics analysis using ANSYS® software [20]. These are followed by evaluation of the obtained results against requirements of an aerial crane operation and repeating these steps until most optimized part is obtained. Fig. 3 shows the road map of the methodology.

Figure 3 here

Figure 3. Roadmap of methodology

2.1. CAD Modeling

The development of CAD model includes building of 3D models using SolidWorks® CAD package. Various parts are built as shown in Fig. 4. All of these parts meet the dimensions stated earlier. Multiphysics analysis is conducted using ANSYS® Multiphysics package [21]. Two types of boundary conditions are applied, that are displacement constraint and distributed forces (pressure). The forces are equally distributed in each sling line and applied on the edge of each sling hole. The boundary conditions are illustrated in Fig. 5.

Figure 4 (a) here	Figure 4 (b) here
Figure 4 (c) here	Figure 4 (d) here

Figure 4. Various 3D parts built in SolidWorks® [9] for the attachment plate.

Figure 5 here

Figure 5. Boundary conditions applied to the model. (a) Displacement constraint applied at the connection between helicopter and the attachment plate. (b) Distributed load (pressure) is applied at the sling holes.

2.2. Multiphysics Analysis

The Multiphysics analysis is performed by applying linear, elastic, isotropic and homogeneous materials. The list of materials used are given in table 1. The von-Mises yield criterion [22][23] is employed for detecting the failure. The use of isotropic model for composite materials is inappropriate; however, one of the requirement is to have effective stresses as low as one-third of the yield strength (factor of safety equal to three). At low values of effective stresses, von-Mises criterion is close to Tsai-Wu criterion [24] which is valid over anisotropic materials such as carbon reinforced fiber polymer (CRFP) [25].

Table 1. Properties of materials; yield strengths, densities and specific strengths.

Table 1 here

2.3. Design optimization

The designs shown in Fig. 4 show high stresses in the sharp corners [26][27]. This clearly indicates that sharp corner produces stress concentration points which must be avoided [28]. It is also realized that the problem is analogous to a simple bending beam considering that the attachment plate is quad symmetric. Solution to such a problem can be found by applying Euler-Bernoulli bending theory [29] [30]. The Euler-Bernoulli equation for the quasi-static bending of slender, isotropic and homogeneous beams under a transverse load is given in Eq. 1.

$$\frac{d^2}{dx^2}\left(EI\frac{d^4w(x)}{dx^4}\right) = EI\frac{d^4w(x)}{dx^4} = q(x) \quad (1)$$

Where x is a unit dimension in longitudinal direction, q(x) is a distributed load, E is the Young's Modulus, I is the area moment of inertia and w(x) is the deflection from the neutral axis of the beam. Similarly, bending moment M(x) and shear force Q(x) can also be expressed in terms of Young's Modulus E, the area moment of inertia I and deflection w(x) as given in Eq. 2 and Eq. 3 [29][30]. Similar design optimization studies have been performed by [31].

$$M(x) = -EI\left(\frac{d^2w(x)}{dx^2}\right) \quad (2)$$

$$Q(x) = = -EI\left(\frac{d^3w(x)}{dx^3}\right) = \frac{dM(x)}{d(x)} \quad (3)$$

2.4. CFRP Samples

The material of choice is CRFP, since it has the highest strength to weight ratio [32][33]. For this study, quasi-isotropic shell structures are made by strengthening fibers in all respective 45∘ angles. A quasi-isotropic shell structure consists of a lay-up of laminates at 0∘, +45∘, +90∘, −45∘ (135∘), 0∘, and so on as shown in Fig. 6. This makes the composite shell structure equally strong in two-dimensional (2D) plane. Different strengths and mechanical properties can be obtained by laying fabrics in different angular positions [34]. This is useful if required in particular application [35].

Figure 6 here

Figure 6: A 3D model showing a quasi-isotropic lay-up of carbon fiber fabrics

In this work, carbon fiber reinforced polymers (CFRPs) shell specimens are fabricated using Multipreg E720 laminates [36]. These laminates consist of two main components,(*Adhesive Film Ef72, "A. Composites*, 2010)(*Syntatic Epoxy Resin Film SC72A*, 2009). The matrix material (also known as resin) is

an adhesive material, which helps to glue carbon fiber fabrics together. The matrix material also aids in increasing the stiffness and strength of the composite material. A generic tensile stress/strain behavior of fibers, resin, and composite is given in Fig. 7 [39]. The failure mechanism of composite material is given by [24].

Figure 7 here

Figure 7**:** A stress/strain diagram, showing the fiber sheets in green, the resin (matrix) material in yellow, and the combined composite material (PMC) in the middle [16].

2.5. Shock Tube Experiment Setup

The shock tube consists of two main parts: the driver section and the driven section (Fig. 8) [40]. The driver section contains compressed air, which is released into the driven section in order to create a shock wave [41]. This is generally triggered with a burst plate or a high speed valve. In given experiments, shock wave is generated in water by releasing high pressure air through high speed valve [6]. The shock wave propagates through water in the driven section [17]. At the end of the driven section, a T-section is fitted, enabling a secure mount of a test specimen (Fig. 9). In these experiments, three pressure sensors (one static and two piezoelectric sensors) are placed at three different places in the shock tube to capture the propagation of the shock wave. The test specimen is mounted with a rosette strain gauge in order to capture the small strains created by the shock wave impact (Fig. 9 and 10).

Figure 8 here

Figure 8: The shock tube. Driver section to the right (containing compressed air) and driven section to the left containing uncompressed water and a T-section for mounting the test specimen.

Figure 9 here	Figure 10
Figure 9: Rosette strain gauge attached to a CRFP specimen using cyanide-based glue. The three-colored wires are connections to three strain gauges at 45◦ angles. The strain gauge is placed in the geometric center of the plate.	Figure 10: The T-section. The CRFP specimen is mounted on the T-section where the three-colored wires are the connection of the rosette strain gauge.

2.6. Material Test System (MTS)

The Material Test System (MTS) is employed to examine the change in properties of test specimens[42][43]. Given setup (Fig. 11) can apply static and dynamic loads up to 100 metric tons. These tests were performed on specimens with and without being subjected to shock impact (Fig. 12).

Figure 11 here	Figure 12 here
Figure 11: The MTS during tensile testing of a steel sample.	Figure 12: Kevlar, CRFP, and aluminum test samples. The ends are reinforced using aluminum plates for holding into the clamps. Rosette strain gauge is mounted for measuring the local strains.

Two kinds of tests were performed using MTS system: tensile (Fig. 13) and flexural tests (Fig. 14). Rosette strain gauges were attached to the middle of each test piece for local strain. An average displacement gauge was also added to measure the total displacement of the test piece. The MTS was pre-programmed to apply tensile load, thus stretching the test piece until it ruptured. Tensile tests proved to be useful; however, clamps may create stress concentration points and hence lead to early failure. This can be avoided by performing flexural tests. Flexural testing is more accurate in order to find the mechanical properties of test specimens.

Figure 13 here	Figure 14 here
Figure 13: Tensile loads applied to a test piece. The material is stretched.	Figure 14: Flexural loads applied to a material. Such load will give a tensile stress in the top surface, a shear stress in the middle, and compressive stresses in the bottom layer.

The experiment has been performed by bending the material using a pressure line in the middle of the test pieces (applied top down), while being placed on two supports (one on the left hand bottom side and one on the right hand bottom side) as shown in Figures 15(a) and 15(b). The middle (top down) line is applying pressure from the top onto the middle of the plane, bending the material until it suffers from total mechanical failure. The test piece used in flexural tests were prepared in the same way as for the tensile tests. In both tests, rosette strain gauge was placed in the geometric center of the test piece. It is expected that the strain

in longitudinal direction (from support to support) is going to be the highest with almost no strain in lateral direction.

Figure 15 (a)	Figure 15 (b)
Figure 15 (a): A sketch of the flexural tests	Figure 15 (b): The actual flexural test performed in MTS

3. RESULTS AND DISCUSSION

3.1. Design Optimization Results

For the beam cross-sections that are symmetrical about the plane parallel to the transverse direction, it can be shown that the bending tensile stress is as given in Eq. 4 [18, 19].

$$\sigma(x) = -Ey\,\frac{d^2w(x)}{dx^2} = \frac{M(x)y}{I} \qquad (4)$$

Where σ(x) is the bending tensile stress and y is a unit dimension in the transverse direction. It is shown from Eq. 4 that the bending tensile stress is directly proportional to the moment. The value of moment is proportional to applied force and distance between the constraint and the loading point. Hence, by reducing the distance between constraint and loading point, the stresses can be reduced. Keeping this in consideration, the models are re-built and tested for stresses. The final optimized three dimensional CAD model of an attachment plate is shown in Fig. 16 (a). Fig. 16 (b) and Fig. 16 (c) show the von-Mises stress and displacement contours. The material of choice is CRFP, since it has the highest strength to weight ratio. The net weight of the optimized model is 0.25 Kg. The maximum stress is about 48 Mpa, which is less than a half to the requirement (one-third of yield strength of CFRP = 107 Mpa; table 1). This gives factor of safety (FOS) of six. Higher FOS is also an advantage against aging failures such as fatigue and creep [28]. Maximum displacement is about 0.034 mm, which is very small in comparison to the part dimensions.

Figure 16 here

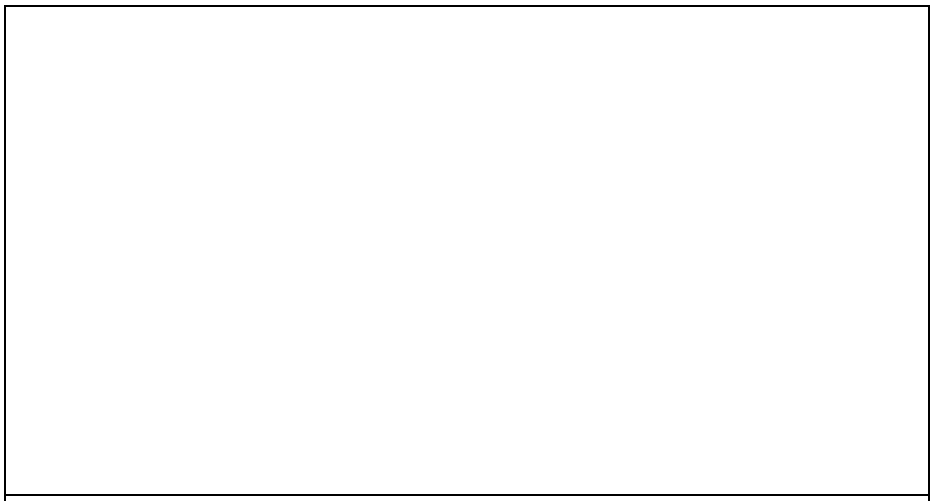

Figure 16 (a): Optimized CAD model.

Figure 16 (b) here

Figure 16 (b): The von-Mises stress (N/m2 = 10-6 Mpa) contours.

Figure 16 (c) here

Figure 16 (c): The resultant displacement (m) contours

3.2. Shock Tube Experiment Results

It is found that strain profile is linear mapping of driven pressure profile which can be seen from Figures 17(a) and 17(b). The experiments are repeated on the same test piece to confirm the validity of the results. Repeated experiments proved that CRFP test pieces can withstand shock pressure (Figure 17(a)); however, it is worth noting that applied shock pressure in these experiments did not result in strains for more than 25% of strain limit for rupture. It can be deduced that material behaves linearly under shock pressure loading which is further confirmed using transient FEM simulation by applying driven pressure loading data from shock tube experiments.

Figure 17 (a)	Figure 17 (b)
Figure 17 (a): Driven pressure profile in shock tube.	Figure 17 (b): Rosette strain gauges' response from four layers of CRFP specimen. Noise in strains after 0.16 s is due to experimental setup.

3.3. Material Test System (MTS) Results

At this stage, it is important to see the response of CRFP test samples under slow loading; therefore, MTS tests are employed. At first, tensile tests are performed on samples as shown in Fig. 12 where stress and strain data are recorded as shown in Fig. 18. Tensile test is run until rupture of the test piece. As shown in Figure 18, that CRFP test sample behaved linearly until rupture. The test specimen ruptured after approximately 37.4 seconds, gaining 10.8 milli-strains. The overall Young's modulus is found to be 28.897GPa, whilst the modulus according to standard is provided as 26.751GPa. A slight deviation is observed in results with repetition in the tests for which a likely cause is variation in the curing process in preparation of the samples. Further, to confirm the linearity of CRFP response, flexural tests (Figures 15(a) and 15(b)) are performed in MTS. The results show the strains in 0∘ (*X*), 45∘ (*XY*), and 90∘ (*Y*) directions. The *X*-strain is largest (red), followed by the *XY* strain (green), and the smallest is the *Y*-strain (blue) as shown in Fig 19. The *X*-strain shows a maximum of 0.013 before the material ruptured after 298 seconds. This shows that the quasi-isotropic CRFP test specimen behaves linearly during low velocity, dynamic loads.

Figure 18 here	Figure 19 here
Figure 18: Stress/strain curve from the initial tensile tests on CRFP test specimens. The test piece ruptured after 37.4 seconds, gaining a strain of 10.8 millistrains in total.	Figure 19: Strains over time gathered during flexural testing. *X* strain in red, *XY*-strain in green, and *Y*-strain in blue. *X*-strain is the largest strain, *XY*-strain is about half of *X*-strain and *Y*-strain is the least.

3.4. Finite Element Method Simulations Results

The FEM simulations are performed using experimental data gathered from shock tube experiments and the MTS, similar study is performed by [44][43]. The 8-node 281-shell element provided in ANSYS 14.0 is used[21]. Mesh sensitivity analysis is carried out to ensure the quality of simulation results. In the analysis, the maximum strain is monitored with the mesh density. The value of maximum strain stabilizes with the increase in mesh density as shown in Fig. 20. The FEM mesh used in simulation is shown in Fig. 21. This represents the FEM model of 1200 elements (mesh density of "4x" from Fig. 20). The simulated shell structure is 2.145mm thick and 3.70 cm in diameter. The outer edges of the circular mesh are constrained in all degrees of freedom (DOFs). Transient pressure data from shock wave experiments is applied to the surface area. Obtained results are shown in Figure 22. The strains obtained from simulations are one-to-one mapping to the pressure data and strain, confirming the results earlier seen in experiments. This demonstrates that there is a coherent response in the structure with the application of dynamic loading.

Thus, the simulations also confirm that the response is linear during transient impulsive loading for quasi-isotropic CRFP.

Figure 20 here	Figure 21 here
Figure 20: Results from the mesh sensitivity analysis (x = 300 elements).	Figure 21: Mesh used in finite element analysis; shown is "4x" mesh density containing 1200 elements.

Figure 22 here
Figure 22: Pressure from experiment compared to equivalent strains from numerical simulation for an eight-layer CRFP.

4. CONCLUSION

Given chapter presents an optimization of an attachment component of a loading hanger with set of requirements. The optimization methodology is a cyclic iterative process. Computer aided design (CAD) model and Multiphysics analysis (for example: finite element methods (FEM)) are the key inputs for the optimization process. CFRPs is the material of choice based on higher strength and light-weight properties. Results from the shock tube experimental setup, Material Test System (with both tensile and flexural testing), and the Finite Element Method simulations using ANSYS software proved that, under dynamic loading, CFRPs E720 composite behaves linearly. A good agreement between simulations and experimental results confirms that Finite Element Method can be used for modelling of deforming structures under dynamic loading especially in the case as that discussed. The results from the given case prove that the mechanical behavior for quasi-isotropic CFRPs E720 laminates is as similar during high speed, short time dynamic shock wave loads as it is for long time static, low velocity loads.

5. REFERENCES

[1] T. Lancashire, *Investigation of the Mechanics of Cargo Handling by Aerial Crane-type Aircraft*. Defense Technical Information Center, 1996.

[2] L. F. Webster, *The Wiley Dictionary of Civil Engineering and Construction*. Wiley, 1997.

[3] V. V. S. K.C. Arora, *Aspects of Materials Handling*. USP/Laxmi Publications (P) Ltd, 2015.

[4] I.H.S.A., *Construction Health and Safety Manual*. Infrastructure Health & Safety Association, 2007.

[5] H. Xue, H. Khawaja, and M. Moatamedi, "Multiphysics design optimization for aerospace applications: Case study on helicopter loading hanger," *AIP Conf. Proc.*, 2014, doi: http://dx.doi.org/10.1063/1.4904695.

[6] H. A. Khawaja, R. Messahel, B. Ewan, S. Mhamed, and M. Moatamedi, "Experimental and Numerical Study of Pressure in a Shock Tube," *J. Press. Vessel Technol. Trans. ASME*, vol. 138, no. 4, Aug. 2016, doi: 10.1115/1.4031591.

[7] H. Xue, H. Khawaja, and M. Moatamedi, "Conceptual design of high speed supersonic aircraft: A brief review on SR-71 (Blackbird) aircraft," in *AIP Conference Proceedings*, Dec. 2014, vol. 1637, no. 1, pp. 1202–1210, doi: 10.1063/1.4904694.

[8] H. Khawaja and M. Moatamedi, "Selection of high performance alloy for gas turbine blade using multiphysics analysis," *Int. J. Multiphys.*, vol. 8, no. 1, pp. 91–100, Mar. 2014, doi: 10.1260/1750-9548.8.1.91.

[9] D. H. andT. W. Clyne, *An Introduction to CompositeMaterials*. Cambridge University Press, Cambridge, UK, 1996.

[10] Meyers, *Shock Wave and High-Strain-Rate Phenomena in Materials,*. CRC Press (Taylor & Francis), 1992.

[11] R. H. Cole, *Underwater Explosions*. Princeton Univ. Press, 1948.

[12] C. Sulfredge, R. Morris, R. S.-P. of the American, and U. 2005, "Calculating the effect of surface or underwater explosions on submerged equipment and structures," *Citeseer*, 2005.

[13] Y. Kim and S. Itoh, "A study on the behavior of underwater shock waves generated in a water

container and its application to magnetic refrigeration material," *Int. J. Multiphys.*, vol. 1, no. 3, pp. 291–302, 2007, doi: https://doi.org/10.1260/175095407782219265.

[14] Y. Nishimura, N. Kawaji, and S. Itoh, "Numerical Analysis of the Behavior of Shock Wave in Spheroid Vessel," *Int. J. Multiphys.*, vol. 4, no. 4, pp. 317–328, 2010, doi: https://doi.org/10.1260/1750-9548.4.4.317.

[15] S. Y. Knyazeva and V. K. Kedrinskiy, *Hydrodynamics of Explosion: Experiments and Models*. Springer, New York, NY, USA, 2006.

[16] A. C. Courtney, L. P. Andrusiv, and M. W. Courtney, "Oxy-acetylene driven laboratory scale shock tubes for studying blast wave effects," *Review of Scientific Instruments*, vol. 83, no. 4. Apr. 2012, doi: 10.1063/1.3702803.

[17] H. Ji, M. Mustafa, H. Khawaja, and M. Moatamedi, "Design of water shock tube for testing shell materials," *World J. Eng.*, vol. 11, no. 1, pp. 55–60, 2014, doi: http://dx.doi.org/10.1260/1708-5284.11.1.55.

[18] P. R. Hampson and M. Moatamedi, "A review of composite structures subjected to dynamic loading," *International Journal of Crashworthiness*, vol. 12, no. 4. pp. 411–428, 2007, doi: 10.1080/13588260701483334.

[19] "Systèmes, D., SolidWorks®," 2012.

[20] "ANSYS®, Academic Research, release 14.0," 2014.

[21] "ANSYS®, Academic Research, Theory Reference, in Structures, Static Analysis release 14.0.," 2014.

[22] R. v. Mises, "Mechanik der festen Körper im plastisch- deformablen Zustand," *Nachrichten von der Gesellschaft der Wissenschaften zu Göttingen, Math. Klasse*, vol. 1913, pp. 582–592, 1913.

[23] R. D. and W. C. Y. Cook, *Advanced mechanics of materials*. Prentice Hall, 1999.

[24] S. W. Tsai and E. M. wu, "A General Theory of Strength for Anisotropic Materials," *J. Compos. Mater.*, vol. 5, no. 1, pp. 58–80, 1971, doi: 10.1177/002199837100500106.

[25] S. Oller, E. Car, J. L.-C. methods in applied mechanics And, and U. 2003, "Definition of a general implicit orthotropic yield criterion," *Elsevier*, 2003.

[26] H. Khawaja, "Application of a 2-D approximation technique for solving stress analyses problem in FEM," *Int. J. Multiphys.*, vol. 9, no. 4, pp. 317–324, Dec. 2015, doi: 10.1260/1750-9548.9.4.317.

[27] H. Khawaja, "Applicability extent of 2-D heat equation for numerical analysis of a multiphysics problem," *AIP Conf. Proc.*, vol. 1798, 2017, doi: 10.1063/1.4972667.

[28] J. and B. G. Gere, *Mechanics of Materials*, SI Edition. Cengage Learning, 2017.

[29] J. M. and S. T. Gere, *Mechanics of materials*. PWS-KENT Pub. Co, 1990.

[30] S. P. Timoshenko, *History of Strength of Materials: With a Brief Account of the History of Theory of Elasticity and Theory of Structures*. Dover Publications, 1983.

[31] Khawaja, Raouf, Parvez, and Scherer, "Optimization of elstomeric micro-fluidic valve dimensions using non-linear finite element methods," *Int. J. Multiphys.*, vol. 3, no. 2, pp. 187–200, Jul. 2009, doi: 10.1260/175095409788837847.

[32] C. H. Strand, Z. Andleeb, and H. A. Khawaja, "Multiphysics Impact Analysis of Carbon Fiber

Reinforced Polymer (CFRP) Shell," *Explos. Shock Waves High Strain Rate Phenom.*, vol. 13, pp. 115–120, 2019, doi: 10.21741/9781644900338-20.

[33] Z. Andleeb, C. Strand, S. Malik, and G. Hussain, "Multiphysics Analysis of CFRP Charpy Tests by varying Temperatures," *Int. J. Multiphys.*, vol. 14, no. 2, pp. 143–160, 2020.

[34] D. C. Barnes, H. ; Stephen, M. Kusek, O. Cross, R. ; Dennis, and A. Lascola, "Quasi-Isotropic Composite Isogrid Structure and Method of Making Same," Google Patent, 1999.

[35] P. D. Soden, M. J. Hinton, and A. S. Kaddour, "Lamina Properties, Lay-up Configurations and loading Conditions for a Range of Fibre-Reinforced Composites Laminates," Google Patent, 1998.

[36] "Multipreg E720, A. Composites," 2010. http://www.ambercomposites.com/.

[37] "Adhesive Film EF72, "A. Composites," 2010. http://www.ambercomposites.com/.

[38] "Synthetic Epoxy Resin Film SC72A," 2009. http://www.ambercomposites.com/.

[39] A. B. Strong, *Fundamentals of Composites Manufacturing, Materials,Methods and Applications, Society ofManufacturing Engineers*, 2nd ed. Dearborn, Mich, USA, 2008.

[40] H. Khawaja, J. Kapaya, and M. Moatamedi, *Shock Tube; Detail overview of equipment and instruments in the shock tube experimental setup*. Lambert Academic Publishing, 2015.

[41] H. A. Khawaja and M. Moatamedi, "Multiphysics investigation of composite shell structures subjected to water shock wave impact in petroleum industry," in *Materials Science Forum*, 2013, vol. 767, pp. 60–67, doi: 10.4028/www.scientific.net/MSF.767.60.

[42] E. Stange, Z. Andleeb, and H. A. Khawaja, "Qualitative visualization of the development of stresses through infrared thermography," *Vestn. MGTU*, vol. 22, no. 4, pp. 503–507, 2019, doi: 10.21443/1560-9278-2019-22-4-503-507.

[43] E. Stange, Z. Andleeb, H. Khawaja, and M. Moatamedi, "Multiphysics study of tensile testing using infrared thermography," *Int. J. Multiphys.*, vol. 13, no. 2, pp. 191–202, 2019, doi: 10.21152/1750-9548.13.2.191.

[44] U. N. Mughal, H. A. Khawaja, and M. Moatamedi, "Finite element analysis of human femur bone," *Int. J. Multiphys.*, vol. 9, no. 2, pp. 101–108, Jun. 2015, doi: 10.1260/1750-9548.9.2.101.